# Evaluating the Crosstalk Current and the Total Radiated Power of a Bent Cable Harness Using the Generalized MTL Method

Yansheng Wang , *Member, IEEE*, Ying S. Cao, *Member, IEEE*, Dazhao Liu, *Member, IEEE*, Richard W. Kautz, Nevin Altunyurt, and Jun Fan , *Fellow, IEEE* 

Abstract—This paper presents a general formulation of the generalized multiconductor transmission line (GMTL) method to model a parallel cable harness including straight and bent wires. The parallel cable harness here indicates the uniform crosssectional wire distribution. The GMTL equations are solved recursively based on the perturbation theory. This GMTL method facilitates an accurate evaluation of the current distributed on a cable harness. On top of that, the current obtained in a radiation problem is decomposed into two traveling currents, i.e., the positive-going and the negative-going currents, based on the leastsquares method. With the decomposed currents, the steepest descent method is further adopted to achieve a fast approximation of the total radiated power. Finally, the capability and the limitations of the GMTL method in terms of the electrical wire separation and length are investigated. The necessity of the recursive corrections is also studied.

*Index Terms*—Cable harness, crosstalk, multiconductor transmission line (MTL), steepest descent (SD) method, total radiated power (TRP).

#### I. INTRODUCTION

ABLE harnesses are widely found in modern transportation systems, such as automobiles [1], high-speed trains [2], aircraft [3], etc. A cable harness is a bundle of wires, which serve as the interconnects among various electronic modules to transmit signals and power. A cable harness needs to be carefully designed and routed in order to meet strict electromagnetic compatibility (EMC) and electromagnetic interference requirements.

To evaluate the design and routing of a cable harness, commonly used metrics include the current distribution, the crosstalk current, the total radiated power (TRP), etc. These metrics can be obtained through either measurements or simulations. However,

Manuscript received June 17, 2018; revised October 13, 2018, February 12, 2019, and June 10, 2019; accepted June 29, 2019. Date of publication July 24, 2019; date of current version August 13, 2020. This work was supported in part by Ford Motor Company and in part by the National Science Foundation under Grant IIP-1440110. (Corresponding author: Jun Fan.)

Y. Wang, Y. S. Cao, D. Liu, and J. Fan are with the Electromagnetic Compatibility Laboratory, Missouri University of Science and Technology, Rolla, MO 65401 USA (e-mail: jfan@mst.edu).

R. W. Kautz and N. Altunyurt are with the Electric Machine Drive Systems Department, Research and Advanced Engineering, Ford Motor Company, Dearborn, MI 48126 USA.

Color versions of one or more of the figures in this paper are available online at http://ieeexplore.ieee.org.

Digital Object Identifier 10.1109/TEMC.2019.2927222

the measurements are usually inconvenient and costly to realize [4], [5]. Simulationwise, a cable harness is usually modeled using either full-wave methods, like method of moments (MoM) [2], [6] and partial element equivalent circuit (PEEC) method [7], or the transmission line (TL) theory [8], [9]. Full-wave methods compute the current distribution on a cable harness with great accuracy, but consume a lot of memory and need long simulation times. An alternative approach to model a cable harness is based on the TL theory. The TL theory simplifies the modeling of a cable harness and the computation of the current distribution.

Over the past decades, several TL-based methods have been developed. Nitsch and Tkachenko[10], [11] derived the fullwave TL theory that could be applied to a set of thin wires. In [12], a generalized TL model was described to study the high-frequency mixed-mode propagation along electrical interconnects. A recursive procedure based on the perturbation theory to evaluate the electric currents and potentials on a single wire above a perfect conducting ground was applied in [13]. The derivation in [14] accounted for the effects of finitely conducting ground on a single wire. An approach was presented in [15] to model the multiconductor transmission line (MTL) with arbitrary terminations; this approach was still applicable even if the TL approximation conditions no longer held. However, all these proposed methods assumed an infinitely large ground plane beneath the wires, which prevents these methods from practical applications, since the reference plane beneath the wires inside a modern transportation system is usually of irregular shape, limited size, and arbitrary discontinuities such as slots, holes, wedges, etc. The methods discussed in [1] and [16]–[18] were not restricted by the reference plane; nevertheless, these papers only derived TL parameters between two conductors. These derivations are not applicable in real situations, where multiple wires exist. The generalized MTL (GMTL) method proposed in [19]–[21] overcame the abovementioned issues by enforcing all wires to refer to infinity. However, all the abovementioned TL-based methods are only applicable for straight wires; these methods do not support bent cable harnesses. To resolve this issue, this paper adopts two analytical methods to extract the per-unit-length (pul) inductance (L) and capacitance (C) of a cable harness, which further enables a general formulation of the GMTL method to cover both straight and bent wires.

0018-9375 © 2019 IEEE. Personal use is permitted, but republication/redistribution requires IEEE permission. See https://www.ieee.org/publications/rights/index.html for more information.

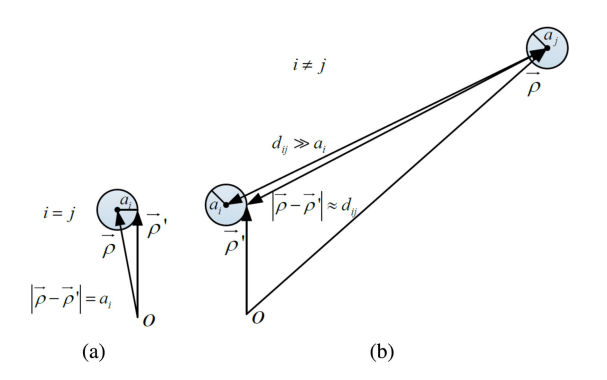


Fig. 1. Cross-sectional geometry for (a) wire i and (b) wires i and j.

With the GMTL method, the distributed current on a cable harness can be obtained. On top of that, it is of great interest to compute the TRP, which evaluates the radiation capability of a radiator [22]. There are several approaches to calculate the TRP of a cable harness. In [23], the Green's function (GF) method was directly applied to compute the radiated field from the distributed current on a cable harness. An integral of the obtained radiated field led to the TRP. The GF method is straightforward, but inefficient. In [24], an efficient TRP calculation method was presented based on the PEEC formulation, where a full inductance and a full capacitance matrices need to be calculated in order to compute the TRP. However, this method cannot be applied in MTL-based formulations, since the inductance and capacitance matrices lack of the mutual terms of wire segments distributed along the wire routing direction in MTL-based formulations. Another approach to compute the TRP was to subtract the ohmic power loss from the input power, which was implemented in EMC studio [25]. This method requires good knowledge of the excitations and the terminations; however, a cable harness, in practice, is terminated by complex loading networks that are difficult to characterize. Therefore, this method is not helpful in real applications. In this paper, an accurate and efficient TRP calculation approach is developed based on the steepest descent (SD) method [26], [28]. In the proposed approach, the obtained current on the cable harness is first approximately decomposed into two traveling currents, i.e., the positive-going (PG) and the negative-going (NG) currents, based on the least-squares method. This current decomposition process is independent of loading conditions, which can be generally applied in any scenario as long as the current on a cable harness is known. Next, the SD method is applied to facilitate the calculation of the radiated field and the TRP. Before this paper, the SD method in terms of TRP calculation was limited to a few simple scenarios like infinitely long wires and two wires with known loadings [26], [28]. This paper proliferates a wide usage of the SD method in radiated field and TRP calculation.

Last but not the least, the capability and limitations of the GMTL method are studied. Though the study focuses on straight cable harnesses, the obtained conclusions generally apply to bent cable harnesses, since they consist of several sections of straight cable harnesses. In the study, two parameters are carefully investigated, i.e., the electrical wire separation and length.

Besides, since the GMTL equations are solved recursively based on the perturbation theory [13], the necessity of the recursive corrections is studied in terms of the accuracy of the crosstalk current and TRP.

The rest of this paper is organized as follows. In Section II, a general formulation of the GMTL method is developed to cover both straight and bent cable harnesses. In Section III, the TRP from an arbitrary cable harness is approximated based on the SD method. In Section IV, the capability and limitations of the GMTL method are discussed. Conclusions are presented in Section V.

# II. GENERAL FORMULATION OF THE GMTL METHOD FOR AN ARBITRARY CABLE HARNESS

In this section, two analytical methods to extract the pul L and C are presented first. The general formulation of the GMTL method for one bent wire is then introduced. After that, the general GMTL formulation is extended to multiwire structures.

#### A. Analytical pul L and C Extraction

In this paper, the two analytical methods to extract the pul *L* and *C* are named two-dimensional (2-D) static and 2-D dynamic pul *L* and *C*, respectively.

1) 2-D Static pul L and C: The 2-D static GF between wires #i and #j reads

$$g_{ij}^{\text{static}}(\overrightarrow{\rho}, \overrightarrow{\rho}') = -\frac{1}{4\pi} \ln |\overrightarrow{\rho} - \overrightarrow{\rho}'|^2 = -\frac{1}{4\pi} \ln \rho_{ij}^2 \qquad (1)$$

where  $\overrightarrow{\rho}$  and  $\overrightarrow{\rho}'$  are the locations of the observation and the source points, respectively. As shown in Fig. 1, we have

$$\rho_{ij} = |\overrightarrow{\rho} - \overrightarrow{\rho}'| = \begin{cases} a_i, & i = j \\ d_{ij}, & i \neq j \end{cases}$$
 (2)

where  $a_i$  is the radius of wire #i and  $d_{ij}$  is the center-to-center separation between wires #i and #j.

The element in the pul inductance matrix  $\overline{L}$ ,  $L_{ij}$ , is derived from the magnetic potential as

$$A_{i}(\overrightarrow{\rho}) = \mu \int_{C} J_{j}(\overrightarrow{\rho}') g_{ij}^{\text{static}}(\overrightarrow{\rho}, \overrightarrow{\rho}') ds$$

$$= \mu \int_{0}^{2\pi} \frac{I_{j}}{2\pi a_{j}} \left( -\frac{1}{4\pi} \ln \rho_{ij}^{2} \right) a_{j} d\theta$$

$$= L_{ij}^{\text{static}} I_{j}$$
(3)

where

$$L_{ij}^{\text{static}} = -\frac{\mu}{4\pi} \ln \rho_{ij}^2. \tag{4}$$

Note that a thin-wire approximation is used here so that the current  $I_j$  flowing on wire #j is uniformly distributed around the wire surface, i.e., the line current density is  $J_j(\overrightarrow{\rho}') = \frac{I_j}{2\pi d_s}$ .

The pul capacitance matrix  $\overline{\overline{C}}$  is the inverse of the pul electric potential coefficient matrix  $\overline{\overline{K}}$ , i.e.,

$$\overline{\overline{C}} = \overline{\overline{K}}^{-1}.$$
 (5)

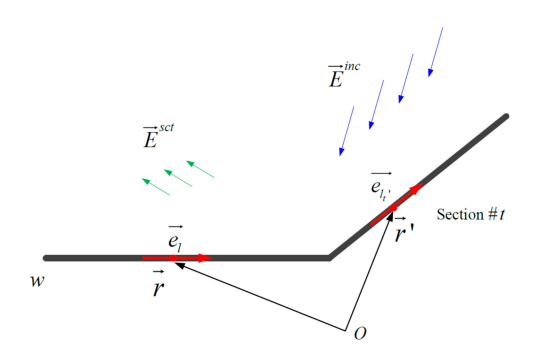


Fig. 2. Single wire illuminated by an incident *E*-field.

The element of  $\overline{\overline{K}}$ ,  $K_{ij}$ , is derived from the electric potential as

$$\phi_{i}(\overrightarrow{\rho}) = \frac{1}{j\omega\varepsilon} \int_{C} \frac{dJ_{j}(\overrightarrow{\rho}')}{dl'} g_{ij}^{\text{static}}(\overrightarrow{\rho}, \overrightarrow{\rho}') ds$$

$$= \frac{1}{j\omega\varepsilon} \int_{0}^{2\pi} \frac{1}{2\pi a_{j}} \frac{dI_{j}}{dl'} \left( -\frac{1}{4\pi} \ln \rho_{ij}^{2} \right) a_{j} d\theta$$

$$= \frac{1}{j\omega} K_{ij}^{\text{static}} \frac{dI_{j}}{dl'}$$
(6)

where l' is the current flowing direction, which is perpendicular to the cross section of the wires, and

$$K_{ij}^{\text{static}} = -\frac{1}{4\pi\varepsilon} \ln \rho_{ij}^2. \tag{7}$$

2) 2-D Dynamic pul L and C: The 2-D dynamic GF between wires #i and #j reads

$$g_{ij}^{\text{dynamic}}(\overrightarrow{\rho}, \overrightarrow{\rho}') = -j\frac{1}{4}H_0^{(2)}\left(k \mid \overrightarrow{\rho} - \overrightarrow{\rho}'\mid\right)$$
$$= -j\frac{1}{4}H_0^{(2)}\left(k\rho_{ij}\right) \tag{8}$$

where k is the wave number in free space and  $H_0^{(2)}(*)$  is the Hankel function of the second kind. Replacing  $g_{ij}^{\mathrm{static}}(\overrightarrow{\rho},\overrightarrow{\rho}')$  in (3) and (6) with  $g_{ij}^{\mathrm{dynamic}}(\overrightarrow{\rho},\overrightarrow{\rho}')$ , the elements in the 2-D dynamic pul  $\overline{\overline{L}}$  and  $\overline{\overline{K}}$  can be obtained as

$$L_{ij}^{\text{dynamic}} = -j\frac{\mu}{4}H_0^{(2)}\left(\rho_{ij}k\right) \tag{9}$$

and

$$K_{ij}^{\text{dynamic}} = -j \frac{1}{4\varepsilon} H_0^{(2)} \left( \rho_{ij} k \right) \tag{10}$$

respectively.

# B. GMTL Formulation for an Arbitrary Single-Wire Structure

As shown in Fig. 2, an arbitrary single wire is illuminated by an incident electric field (*E*-field)  $\overrightarrow{E}^{inc}$ . For a thin wire in the MoM, the scattered *E*-field is

$$\overrightarrow{E}^{\text{sct}} = -j\omega \overrightarrow{A} - \nabla \phi \tag{11}$$

where the vector magnetic potential  $\overrightarrow{A}$  and the scalar electric potential  $\phi$  are

$$\overrightarrow{A}(\overrightarrow{r}) = \mu \int_{w} i(\overrightarrow{r'}) \overrightarrow{e_{l'}} g(\overrightarrow{r}, \overrightarrow{r'}) dr'$$
 (12)

$$\phi(\overrightarrow{r}) = \frac{1}{\varepsilon} \int_{w} \left( -\frac{1}{j\omega} \frac{d}{dl'} i(\overrightarrow{r'}) \right) g(\overrightarrow{r}, \overrightarrow{r'}) dr'$$
 (13)

the free-space GF  $g(\overrightarrow{r}, \overrightarrow{r}')$  is

$$g(\overrightarrow{r}, \overrightarrow{r}') = \frac{e^{-jkR}}{4\pi R} \tag{14}$$

$$R = |\overrightarrow{r} - \overrightarrow{r}'| \tag{15}$$

w is the integral domain including the location along all wires,  $\overrightarrow{r'}$  and  $\overrightarrow{r'}$  indicate the observation and the source locations, respectively, l' is the local wire direction at the source location  $\overrightarrow{r'}$ , and  $\overrightarrow{e_{l'}}$  is the unit vector along the l'-direction at the source location  $\overrightarrow{r'}$ .

Applying the perfect electric conductor boundary condition on the locally l-directed thin wire leads to

$$E_l^{\text{sct}} = -j\omega A_l - \frac{d\phi}{dl} = -E_l^{\text{inc}}.$$
 (16)

The subscript l in (16) indicates the l component of a quantity. After simple manipulations of (13) and (16), the following equations are obtained:

$$\begin{cases} \frac{d}{dl}\phi + j\omega A_l = E_l^{\text{inc}} \\ \phi + \frac{1}{2\omega}P = 0 \end{cases}$$
 (17)

where

$$A_{l}(\overrightarrow{r}) = \sum_{t=1}^{T} \left( \overrightarrow{e_{l'_{t}}} \cdot \overrightarrow{e_{l}} \right) \mu \int_{w_{t}} i(\overrightarrow{r}') g(\overrightarrow{r}, \overrightarrow{r}') dr' \qquad (18)$$

T is the total straight sections constituting an arbitrary cable harness, t indicates the #t straight section,  $w_t$  indicates the #t integral domain out of the total integral domain w,  $\overrightarrow{e_{l'}}$  is the unit vector along the l'-direction at the source location  $\overrightarrow{r'}$  in  $w_t$ ,  $\overrightarrow{e_l}$  is the unit vector along the l-direction at the observation location  $\overrightarrow{r'}$  and

$$P(\overrightarrow{r'}) = \frac{1}{\varepsilon} \int_{sr} \frac{d}{dl'} i(\overrightarrow{r'}) g(\overrightarrow{r'}, \overrightarrow{r'}) dr'. \tag{19}$$

For clear illustrations, only two straight sections are considered in the structures shown in Figs. 2 and 3.

After adding  $j\omega Li$  to both sides of the first equation in (17) and  $\frac{1}{j\omega}C^{-1}\frac{d}{dl}i$  to both sides of the second equation in (17), with some manipulations, the following equations are obtained:

$$\begin{cases} \frac{d}{dl}\phi + j\omega Li = E_l^{\text{inc}} + j\omega D_1 \{i\} \\ \frac{d}{dl}i + j\omega C\phi = D_2 \{i\} \end{cases}$$
 (20)

where

$$D_1\left\{i\right\} = Li - A_l \tag{21}$$

$$D_2\{i\} = \frac{d}{dl}i - CP \tag{22}$$

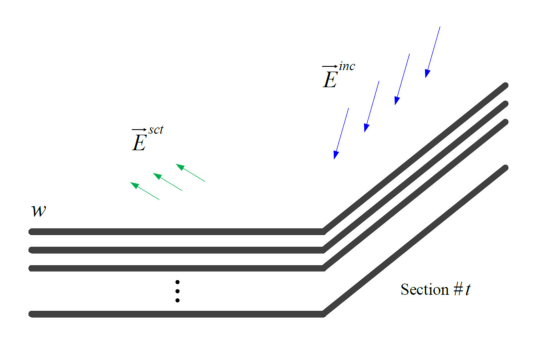


Fig. 3. Multiwire structure illuminated by incident *E*-field.

and L and C are the analytical pul L and C, respectively, i.e.,  $(L,C) \in \{(L^{\text{static}},C^{\text{static}}),(L^{\text{dynamic}},C^{\text{dynamic}})\}.$ 

#### C. Extension to a Multiwire Structure

Adopting the extracted analytical pul  $\overline{\overline{L}}$  and  $\overline{\overline{C}}$ , the following equations are constructed to compute the current distribution on an arbitrary wire structure consisting of N wires:

$$\begin{cases}
\frac{d}{dl}\overline{\phi} + j\omega\overline{\overline{L}}i = \overline{E}_l^{\text{inc}} + j\omega\overline{D}_1\{\overline{i}\} \\
\frac{d}{dl}\overline{i} + j\omega\overline{\overline{C}}\phi = \overline{D}_2\{\overline{i}\}
\end{cases}$$
(23)

where the electric potential  $\phi$ , the current i, and the l-component of the incident E-field  $E_l^{\rm inc}$  in vector format are

$$\overline{\phi} = \begin{bmatrix} \phi_1 \\ \phi_2 \\ \vdots \\ \phi_N \end{bmatrix}, \overline{i} = \begin{bmatrix} i_1 \\ i_2 \\ \vdots \\ i_N \end{bmatrix}, \text{ and } \overline{E}_l^{\text{inc}} = \begin{bmatrix} E_{l,1}^{\text{inc}} \\ E_{l,2}^{\text{inc}} \\ \vdots \\ E_{l,N}^{\text{inc}} \end{bmatrix},$$

respectively. The source correction terms

$$\overline{D}_1\left\{\overline{i}\right\} = \overline{\overline{L}i} - \overline{A}_l \tag{24}$$

and

$$\overline{D}_2\left\{\overline{i}\right\} = \frac{d}{dl}\overline{i} - \overline{\overline{C}P} \tag{25}$$

in (23) are used to compensate the formulation difference between the rigorous MoM and the TL-like method. The nth elements in  $\overline{A}_l$  and  $\overline{P}$  at the observation location  $\overrightarrow{r}$  are computed as

$$A_{l,n}(\overrightarrow{r}) = \sum_{t=1}^{T} \left( \overrightarrow{e_{l'_t}} \cdot \overrightarrow{e_l} \right) \mu \int_{w_t} i(\overrightarrow{r'}) g(\overrightarrow{r'}, \overrightarrow{r'}) dr' \qquad (26)$$

and

$$P_n(\overrightarrow{r}) = \frac{1}{\varepsilon} \int_{w} \frac{d}{dl'} I(\overrightarrow{r}') g(\overrightarrow{r}, \overrightarrow{r}') dr'$$
 (27)

respectively, and n indicates wire #n. Note that the integral domain  $w_t$  includes all the N wires in the #t section.

The perturbation theory [13] is applied to solve (23). The beginning (n=0) results  $\overline{\phi}_{(0)}$  and  $\overline{I}_{(0)}$  are obtained via the

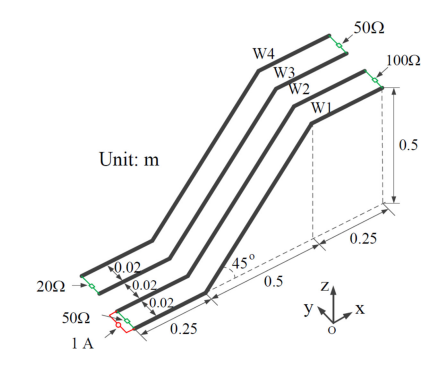


Fig. 4. Bent four-wire structure with three straight sections. "W" denotes wire.

following equations:

$$\begin{cases}
\frac{d}{dl}\overline{\phi}_{(0)} + j\omega\overline{\overline{L}}i_{(0)} = \overline{E}_l^{\text{inc}} \\
\frac{d}{dl}\overline{i}_{(0)} + j\omega\overline{\overline{C}}\overline{\phi}_{(0)} = \overline{0}
\end{cases}$$
(28)

The subsequent  $(n \ge 1)$  electric potential and current perturbations are then obtained by

$$\begin{cases}
\frac{d}{dl}\overline{\phi}_{(n)} + j\omega\overline{\overline{L}}i_{(n)} = j\omega\overline{D}_1\left\{\overline{i}_{(n-1)}\right\} \\
\frac{d}{dl}\overline{i}_{(n)} + j\omega\overline{\overline{C}}\phi_{(n)} = \overline{D}_2\left\{\overline{i}_{(n-1)}\right\}
\end{cases}$$
(29)

The final solutions to (23) are

$$\overline{\phi} = \overline{\phi}_{(0)} + \overline{\phi}_{(1)} + \overline{\phi}_{(2)} + \cdots$$
 (30)

and

$$\bar{i} = \bar{i}_{(0)} + \bar{i}_{(1)} + \bar{i}_{(2)} + \cdots$$
 (31)

## D. Numerical Test Case

A numerical test case is created, as shown in Fig. 4. Lumped circuit elements are added at the cable ends. No perpendicular physical wire segments exist at the cable ends. Equation (23) is applied to compute the current distributed on the wires. Both the static and the dynamic pul L and C are employed to construct the GMTL equations. Correspondingly, they are referred to as the static and the dynamic GMTL, respectively. The computation results are compared in Figs. 5 and 6. In Fig. 5, currents on wires 1 and 3 for a single frequency of 900 MHz are compared. In Fig. 6, currents at the location of x = 0.2 m on wires 1 and 3 for 5–1000 MHz are compared. The initial result indicates the beginning current obtained by the GMTL method without any recursive correction. The final result refers to the finally converged current obtained by the GMTL method after several recursive corrections. To validate the currents obtained by the GMTL method, the mixed-potential integral equation (MPIE, one formulation of the MoM) solver in [20] is used to calculate the current, i.e., the MPIE result serves as the reference. From both Figs. 5 and 6, the beginning current on wire 1 slightly differs from the reference result, and the beginning current on wire 3 significantly deviates from the reference result. With two recursive corrections, the converged result is obtained. The converged currents on wires 1 and 3 match well with the reference. It can be concluded that the general formulation of the GMTL

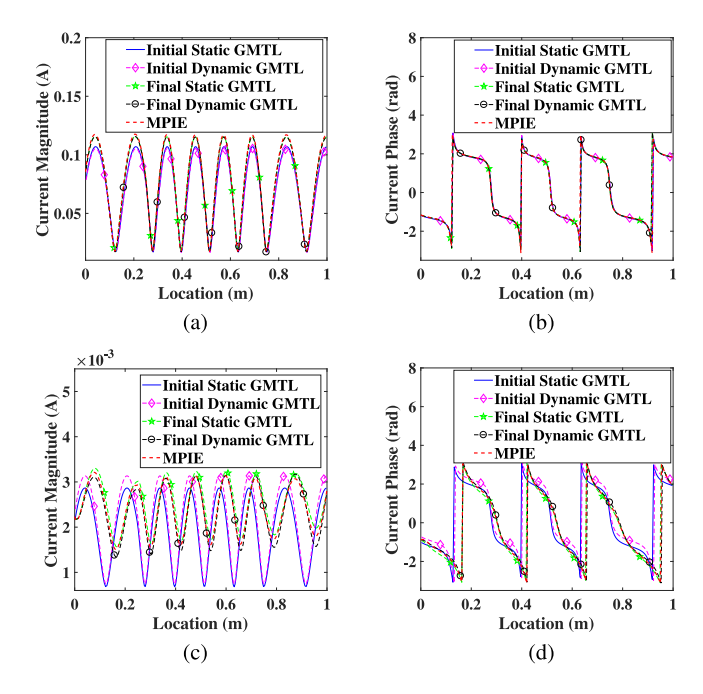


Fig. 5. At 900 MHz, (a) magnitude and (b) phase of the current on Wire 1, and (c) magnitude and (d) phase of the current on Wire 3.

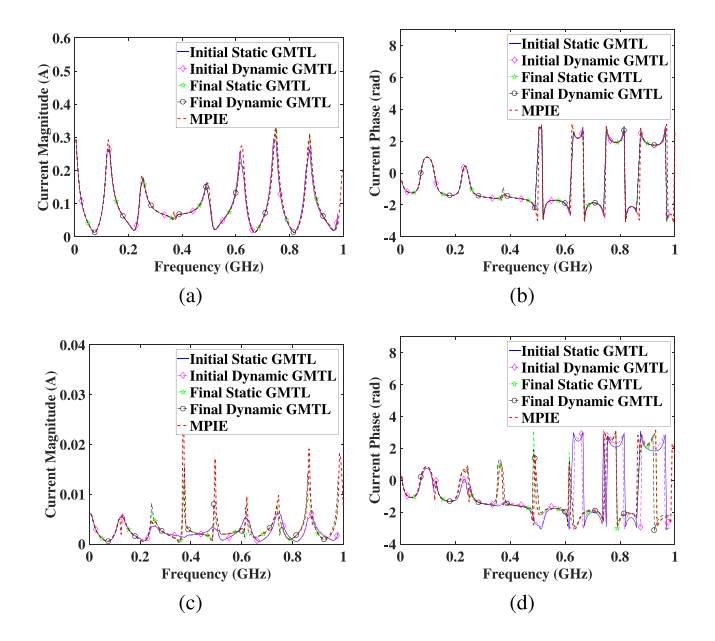


Fig. 6. At x = 0.2 m, (a) magnitude and (b) phase of the current on wire 1, and (c) magnitude and (d) phase of the current on wire 3.

method is correct, and that both the static and the dynamic GMTL produce accurate results. Since the static and the dynamic GMTL equivalently reach the same accurate results, only the dynamic GMTL is employed in the following discussions.

# III. TRP CALCULATION BASED ON THE SD METHOD

For TRP calculation, the SD method is superior to the GF method in terms of efficiency [23], [26]. However, there were only limited applications of the SD method for simple structures

like a two-wire structure or a single wire above a large ground plane [23], [26]. The limitation was due to a lack of proper methods to decompose the total current on a multiwire structure with complex termination networks into traveling currents going in opposite directions. In this section, a current decomposition method based on the least-squares method is proposed first. Next, with the decomposed currents, the radiated field and the TRP are approximated using the SD method. A numerical validation follows. In this section, the TRP computed based on the GF method serves as the reference result.

#### A. Current Decomposition

The total current flowing on a cable harness can be decomposed as the traveling modes and the higher order modes. The magnitude of the traveling modes remains the same along the wire, while the higher order modes decay rapidly when running away from the discontinuities such as the wire ends and bends, which is similar to the leaky modes in a conventional two-wire TL [27]. The magnitude of the traveling modes is typically much larger than that of the higher order modes. Therefore, the traveling modes dominate the contribution to the radiated field and the TRP, and the higher order modes can be neglected in terms of TRP calculation. This can be treated as *a posteriori*, which is verified in a later example.

According to the SD method proposed in [28], the total current obtained on each straight section of a wire first needs to be approximately decomposed into two traveling currents: the PG and the NG currents. This is achieved by the method described in the following.

The total current I at the position  $\overrightarrow{r}'$  of a straight section of a wire can be expressed as the summation of the PG and the NG currents, which reads

$$I(\overrightarrow{r}') = I^{+}e^{-j\overrightarrow{\beta}\cdot\overrightarrow{r}'} + I^{-}e^{j\overrightarrow{\beta}\cdot\overrightarrow{r}'}$$
(32)

where  $\overrightarrow{\beta}$  is the vector of propagation constant of the traveling modes, and  $I^+$  and  $I^-$  are the amplitudes of the PG and the NG currents, respectively. Equation (32) holds at all the m source locations, i.e.,  $\overrightarrow{r_1}'$ ,  $\overrightarrow{r_2}'$ , ...,  $\overrightarrow{r_m}'$ , on that straight section of the wire. Arranging (32) in the matrix representation, it reads

$$\overline{\overline{T}} \cdot \overline{c} = \overline{I} \tag{33}$$

where

$$\overline{\overline{T}} = \begin{bmatrix}
e^{-j\overrightarrow{\beta}\cdot\overrightarrow{r_1}'} & e^{j\overrightarrow{\beta}\cdot\overrightarrow{r_1}'} \\
e^{-j\overrightarrow{\beta}\cdot\overrightarrow{r_2}'} & e^{j\overrightarrow{\beta}\cdot\overrightarrow{r_2}'} \\
\vdots & \vdots \\
e^{-j\overrightarrow{\beta}\cdot\overrightarrow{r_m}'} & e^{j\overrightarrow{\beta}\cdot\overrightarrow{r_m}'}
\end{bmatrix}$$
(34)

$$\overline{c} = \begin{bmatrix} I^+ \\ I^- \end{bmatrix} \tag{35}$$

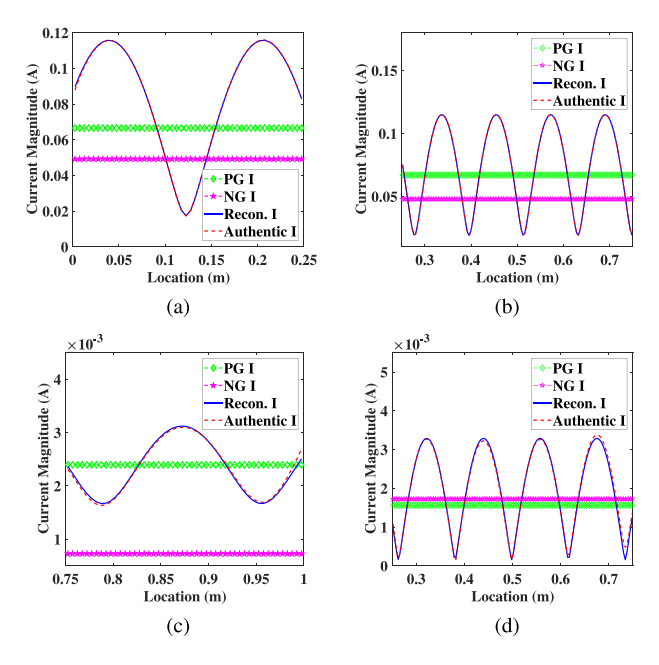


Fig. 7. At 900 MHz, magnitudes of the PG current (PG I), the NG current (NG I), the reconstructed current (Recon. I), and the authentic current (Authentic I) are compared in (a) the first section on wire 1, (b) the second section on wire 2, (c) the third section on wire 3, and (d) the second section on wire 4.

and

$$\overline{I} = \begin{bmatrix}
I(\overrightarrow{r_1}') \\
I(\overrightarrow{r_2}') \\
\vdots \\
I(\overrightarrow{r_m}')
\end{bmatrix}.$$
(36)

The unknown amplitudes  $\bar{c}$  in (33) can be solved using the least-squares method

$$\overline{c} = \left(\overline{\overline{T}}^* \overline{\overline{T}}\right)^{-1} \overline{\overline{T}}^* \overline{I} \tag{37}$$

where \* is the conjugate transpose operator.

Revisiting the test case in Fig. 4, the authentic total current on each section of a wire is decomposed into the PG and the NG currents. The summation of the PG and the NG currents results in the reconstructed total current. All these current quantities are compared in Fig. 7. As shown in the figure, the reconstructed current correlates well with the total current, which demonstrates the feasibility of the least-squares method.

#### B. TRP Approximation Based on the SD Method

Using the SD method in [28], the radiated magnetic field  $H_{\rm rad}$  at the location of  $\overrightarrow{r}$  can be approximated as

$$H_{\rm rad}\left(\overrightarrow{r}\right) \approx \sum_{n=1}^{N} \frac{e^{-jkR}}{4\pi R} U_n \left(A_n + B_n\right)$$
 (38)

where

$$A_n = \frac{\overrightarrow{e_n} \times \overrightarrow{e_R}}{\beta/k - \overrightarrow{e_n} \cdot \overrightarrow{e_R}} I_n^+ e^{-j\overrightarrow{\beta} \cdot \overrightarrow{r_n}'}$$
 (39)

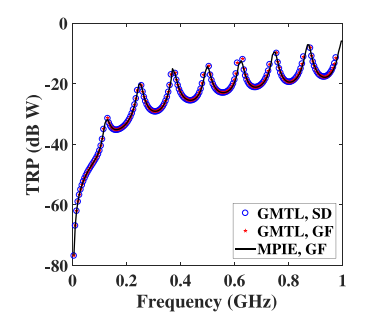


Fig. 8. TRP correlation among different methods.

and

$$B_n = \frac{-\overrightarrow{e_n} \times \overrightarrow{e_R}}{\beta/k + \overrightarrow{e_n} \cdot \overrightarrow{e_R}} I_n^- e^{j\overrightarrow{\beta} \cdot \overrightarrow{r_n'}}.$$
 (40)

In (38), n indicates the nth discontinuity point out of the N total discontinuity points, k is the wave number in free space,  $R=|\overrightarrow{r'}-\overrightarrow{r_n'}|$  is the distance between the observation point  $\overrightarrow{r'}$  and the nth discontinuity point  $\overrightarrow{r_n'}$ , and  $U_n=\pm 1$  at the starting point and the ending point of the PG current, respectively. The observation points  $\overrightarrow{r'}$  locate over a sphere with a radius of  $r_{\rm sph}$  and centered at the geometric center of the cable harness under investigation. The discontinuity points refer to the bent points and the ends of the cable harness. In (39) and (40),  $\overrightarrow{e_n}$  is the unit direction vector of the PG current,  $\overrightarrow{e_R}$  is the unit direction vector from the nth discontinuity point  $\overrightarrow{r_n'}$  to the observation point  $\overrightarrow{r}$ , and  $I_n^+e^{-j\overrightarrow{\beta}\cdot\overrightarrow{r_n'}}$  and  $I_n^-e^{j\overrightarrow{\beta}\cdot\overrightarrow{r_n'}}$  are the PG and the NG currents at the nth discontinuity point  $\overrightarrow{r_n'}$ , respectively.

Furthermore, the TRP is calculated using

$$TRP = \iint_{\Omega} \frac{r_{\rm sph}^2}{2} \eta |H_{\rm rad}|^2 d\Omega \tag{41}$$

where  $\Omega$  is the solid angle over the whole observation sphere and  $\eta$  is the wave impedance in free space.

#### C. Numerical Validation

Revisiting the test case in Fig. 4, the current distributed on the cable harness is obtained by sweeping the frequency from 5 to 1000 MHz. The SD and the GF methods are applied to the GMTL current to compute the TRP. As a reference, the GF method is also employed in the MPIE current to compute the TRP. The obtained TRPs are shown in Fig. 8. TRPs obtained by all these three approaches correlate very well, which validates the proposed TRP calculation method.

#### IV. CAPABILITY AND LIMITATIONS OF THE GMTL METHOD

In this section, the capability and limitations of the GMTL method are investigated via two parameters, the electrical wire separation and length. Also, the necessity of the recursive corrections is studied. Though the study is based on straight cable harnesses, the conclusions can be naturally applied to bent cable harness since they consist of several sections of straight cable harnesses.

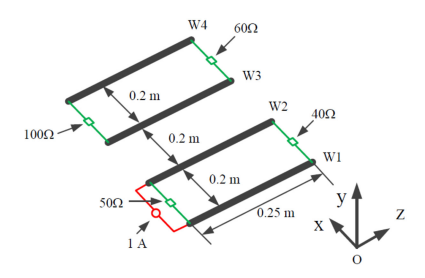


Fig. 9. Four-wire case to study the electrical wire separation.

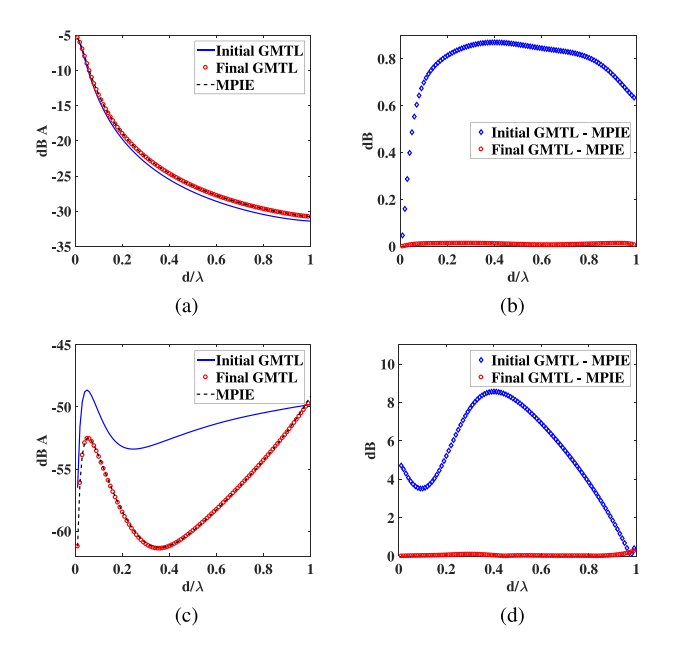


Fig. 10. Current magnitude comparison at the center of wire 1: (a) the absolute value and (b) the difference. Current magnitude comparison at the center of wire 3: (c) the absolute value and (d) the difference.

## A. Electrical Wire Separation

The electrical wire separation is defined using the ratio of the maximal wire separation d over the wavelength  $\lambda$ , i.e.,  $d/\lambda$ . A case is created to investigate how the current distribution and the TRP are affected by the electrical wire separation. Detailed geometry, excitation, and termination of this case are provided in Fig. 9. In this case, the maximal wire separation is 0.6 m, i.e., d=0.6.

As the frequency is swept, the current magnitudes at the center of wires 1 and 3 are recorded. The obtained currents are compared in Fig. 10. The legend in the figure is explained as follows. The initial GMTL indicates the GMTL method without any recursive correction. The final GMTL refers to the GMTL method with several recursive corrections to ensure a converged current. The MPIE stands for the reference method [20]. Fig. 10(b) and (d) each has two curves. The diamond line refers to the absolute current difference between the initial GMTL and the MPIE. The circle line refers to the absolute current difference between the final GMTL and the MPIE.

As shown in Fig. 10(b) and (d), as the electrical wire separation increases, current by the initial GMTL generally differs

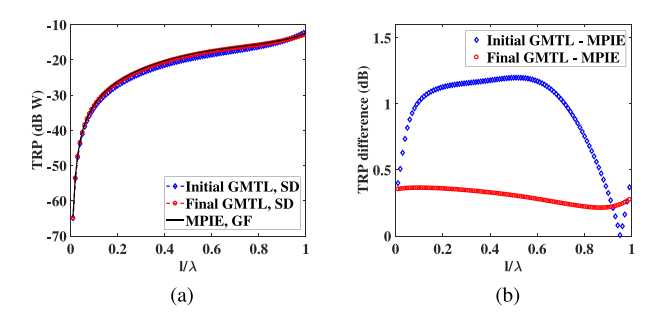


Fig. 11. TRP comparison. (a) Absolute value. (b) Difference.

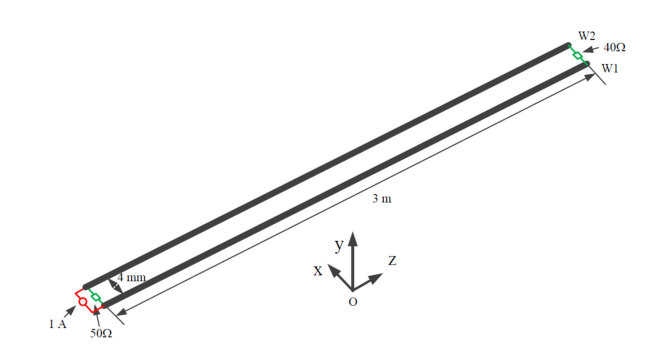


Fig. 12. Two-wire case to study the electrical wire length.

from the one by the MPIE. After two recursive corrections, current by the final GMTL matches well with the one by the MPIE. As shown in Fig. 10(b), the current difference between the initial GMTL and the MPIE on wire 1 is less than 1 dB, which is negligible. However, the current difference between the initial GMTL and the MPIE on wire 3 (crosstalk current) is mostly larger than 3 dB, as shown in Fig. 10(d), which cannot be ignored. Therefore, if the crosstalk current is of great interest, the recursive correction is required to reach an accurate result.

As shown in Fig. 11, as the electrical wire separation increases, the TRPs of the initial GMTL and the final GMTL are similar to the reference TRP. The maximal TRP difference is between the initial GMTL and the MPIE, and it is less than 1.5 dB, a negligible difference. Generally speaking, if the TRP is the major concern, there is no need to conduct recursive corrections.

#### B. Electrical Wire Length

The electrical wire length is defined as the ratio of the wire length l over the wavelength  $\lambda$ , i.e.,  $l/\lambda$ . A case is created to study how the current distribution and the TRP are affected by the electrical wire length. Detailed geometry, excitation, and termination of this case are provided in Fig. 12. In this case, the wire length is 3 m, i.e., l=3, which equals 20 wavelengths at 2 GHz. The wire separation is 4 mm, which is less than 1/30 wavelength at 2 GHz. Therefore, the effects due to the wire separation can be neglected.

As the frequency is swept, the current magnitude at the center of wire 1 is recorded and illustrated in Fig. 13. Fig. 13(a) shows an overview of the result. Fig. 13(b)–(d) shows the enlarged

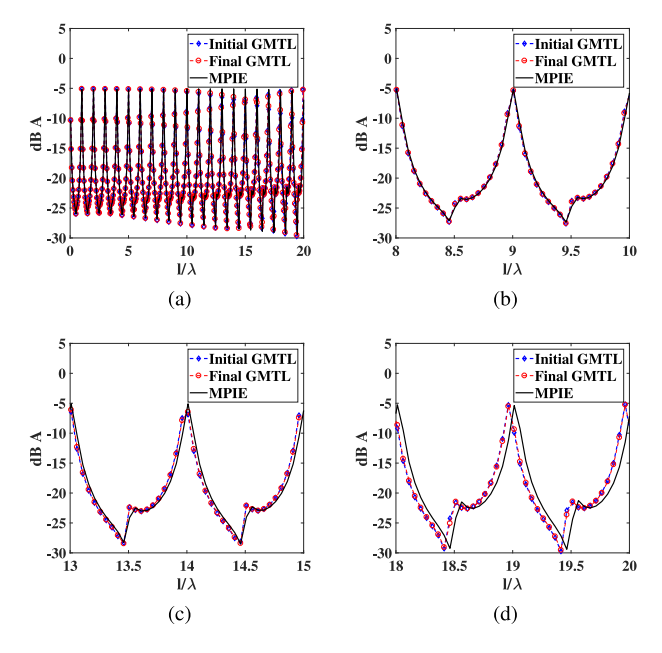


Fig. 13. Current magnitude comparison at the center of wire 1 for different ranges of  $l/\lambda$ . (a)  $0 \le l/\lambda \le 20$ . (b)  $8 \le l/\lambda \le 10$ . (c)  $13 \le l/\lambda \le 15$ . (d)  $18 \le l/\lambda \le 20$ .

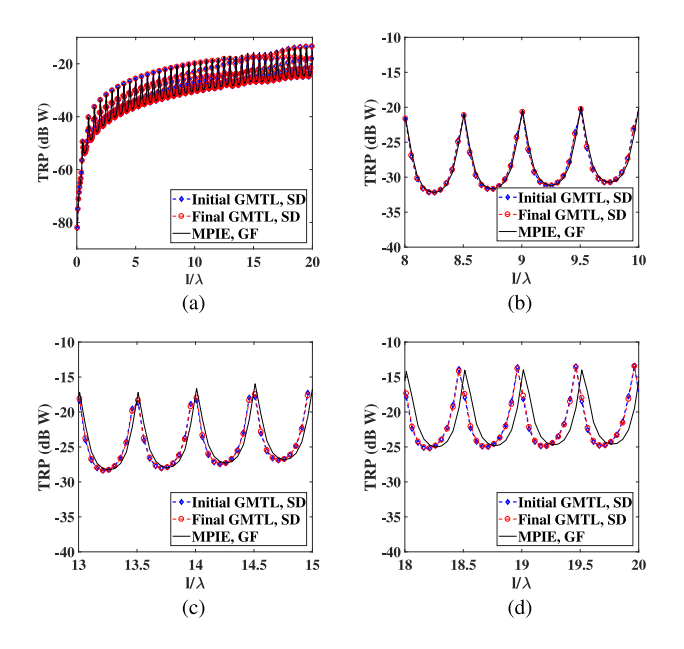


Fig. 14. TRP comparison for different ranges of  $l/\lambda$ . (a)  $0 \le l/\lambda \le 20$ . (b)  $8 \le l/\lambda \le 10$ . (c)  $13 \le l/\lambda \le 15$ . (d)  $18 \le l/\lambda \le 20$ .

portions of Fig. 13(a). In the figure, the current obtained by the GMTL is almost the same as the one obtained by the MPIE when  $l/\lambda \leq 15$ . When  $l/\lambda > 15$ , the shift of resonant frequencies can be obviously observed. A similar trend is found in the TRP comparison, as shown in Fig. 14. When  $l/\lambda \leq 15$ , the TRP of the GMTL is almost the same as the TRP of the MPIE. However, when  $l/\lambda > 15$ , the shift of resonant frequencies can be obviously observed. This shifting of resonant frequencies is due to the mesh size differing from the GMTL to the MPIE.

From Figs. 13 and 14, it can be concluded that along with the increasing electrical wire length, the shifting of the resonant frequencies becomes more and more severe. However, this is still acceptable within 15 wavelengths. Besides, comparing the final GMTL to the initial GMTL, the result improvement due to the recursive corrections is insignificant.

#### V. CONCLUSION

In this paper, a general formulation of the GMTL method is developed for a parallel cable harness, which can be straight or bent. A parallel cable harness indicates the uniform cross-sectional wire distribution. Two analytical methods to extract the pul L and C are derived. Either set of the pul L and C can be used to build the GMTL equations, which produce similar currents. The GMTL equations are solved based on the perturbation theory, though the convergence of the solution is not rigorously demonstrated. Based on experience, the iterative process always converges for nonresonant frequencies of the cable harness. Accurate current distribution on a cable harness is obtained after one or two recursions. The efficiency of the proposed method is not yet proved.

Besides, the TRP of a cable harness with complex loading networks can be conveniently evaluated based on the SD method. To be able to apply the SD method, currents flowing on the cable harness are decomposed into the PG and the NG currents using the least-square method. Once the decomposition is achieved, the decomposed traveling currents at all discontinuity points dominate the contribution to the radiated field. The SD method is more efficient than the GF method in terms of TRP calculation.

Finally, the capability and limitations of the GMTL method are studied in terms of the electrical wire separation and length. It is found that the electrical wire separation does not limit the capability of the GMTL method, and that the GMTL method achieves accurate current and the TRP as the electrical wire separation varies from 0 to 1. When it comes to the electrical wire length, the GMTL method generally works well. However, as the electrical wire length increases, the shifting of the resonant frequencies becomes increasingly severe. From this perspective, the GMTL method is accurate up to a limited number of wavelengths. The necessity of the recursive corrections is also investigated. According to the study, recursive corrections are required in order to achieve accurate crosstalk current. However, if the TRP is the major concern, the obtained result is acceptable even if no recursive correction is added.

The GMTL is an extension of the traditional TL theory. Some limitations in the traditional TL theory may still be applicable in the GMTL approach. As is known, the TL theory fails at wire resonances if TLs are left open without terminations. This limitation is also true for the GMTL approach. To resolve the issue, additional loss terms may be added either lumped at the ends of the wires [29], [30] or distributed along the wires [31]. The present formulation of the GMTL method is based on thin wire assumptions. For thick wire cases where nonuniform current distribution and proximity effects should be considered, the modal decomposition method [32], [33] can be employed to extract pul L and C. The dielectrics and losses of a cable harness are not included in this paper but are studied in progress.

#### REFERENCES

- D. Liu, Y. Wang, R. W. Kautz, N. Altunyurt, S. Chandra, and J. Fan, "Accurate evaluation of field interactions between cable harness and vehicle body by a multiple scattering method," *IEEE Trans. Electromagn. Compat.*, vol. 59, no. 2, pp. 383–393, Apr. 2017.
- [2] D. Zhang, Y. Wen, Y. Wang, D. Liu, X. He, and J. Fan, "Coupling analysis for wires in a cable tray using circuit extraction based on mixed-potential integral equation formulation," *IEEE Trans. Electromagn. Compat.*, vol. 59, no. 3, pp. 862–872, Jun. 2017.
- [3] H. Bagci, A. E. Yilmaz, J. Jin, and E. Michielssen, "Fast and rigorous analysis of EMC/EMI phenomena on electrically large and complex cableloaded structures," *IEEE Trans. Electromagn. Compat.*, vol. 49, no. 2, pp. 361–381, May 2007.
- [4] G. Li et al., "Measurement-based modeling and worst-case estimation of crosstalk inside an aircraft cable connector," *IEEE Trans. Electromagn.* Compat., vol. 57, no. 4, pp. 827–835, Aug. 2015.
- [5] S. Sun, G. Liu, J. L. Drewniak, and D. J. Pommerenke, "Hand-assembled cable bundle modeling for crosstalk and common-mode radiation prediction," *IEEE Trans. Electromagn. Compat.*, vol. 49, no. 3, pp. 708–718, Aug. 2007.
- [6] Y. Wang, R. Kautz, N. Altunyurt, and J. Fan, "An equivalent circuit model for the wire-to-surface junction based on method of moments," in *Proc. IEEE Int. Conf. Wireless Inf. Technol. Syst. Appl. Comput. Electromagn.*, Honolulu, HI, USA, 2016, pp. 1–2.
- [7] J. Nitsch, F. Gronwald, and G. Wollenberg, Radiating Nonuniform Transmissionline Systems and the Partial Element Equivalent Circuit Method. Hoboken, NJ, USA: Wiley, 2009.
- [8] I. Badzagua et al., "Effective computational techniques for EMC analysis of cable harness," in Proc. Int. Seminar/Workshop Direct Inverse Probl. Electromagn. Acoust. Wave Theory, Sep. 2010, pp. 96–102.
- [9] C. R. Paul, Analysis of Multiconductor Transmission Lines, 2nd ed. Hoboken, NJ, USA: Wiley–IEEE Press, Oct. 2007.
- [10] J. B. Nitsch and S. V. Tkachenko, "Complex-valued transmission-line parameters and their relation to the radiation resistance," *IEEE Trans. Electromagn. Compat.*, vol. 46, no. 3, pp. 477–487, Aug. 2004.
- [11] J. B. Nitsch and S. V. Tkachenko, "High-frequency multiconductor transmission-line theory," *Found. Phys.*, vol. 40, no. 9, pp. 1231–1252, 2010
- [12] A. G. Chiariello, A. Maffucci, G. Miano, F. Villone, and W. Zamboni, "A transmission-line model for full-wave analysis of mixed-mode propagation," *IEEE Trans. Adv. Packag.*, vol. 31, no. 2, pp. 275–284, May 2008.
- [13] S. V. Tkatchenko, F. Rachidi, and M. Ianoz, "Electromagnetic field coupling to a line of finite length: Theory and fast iterative solutions in frequency and time domains," *IEEE Trans. Electromagn. Compat.*, vol. 37, no. 4, pp. 509–518, Nov. 1995.
- [14] V. Cooray, F. Rachidi, and M. Rubinstein, "Formulation of the field-to-transmission line coupling equations in terms of scalar and vector potentials," *IEEE Trans. Electromagn. Compat.*, vol. 59, no. 5, pp. 1586–1591, Oct. 2017.
- [15] G. Lugrin, S. V. Tkachenko, F. Rachidi, M. Rubinstein, and R. Cherkaoui, "High-frequency electromagnetic coupling to multiconductor transmission lines of finite length," *IEEE Trans. Electromagn. Compat.*, vol. 57, no. 6, pp. 1714–1723, Dec. 2015.
- [16] A. Maffucci, G. Miano, and F. Villone, "An enhanced transmission line model for conducting wires," *IEEE Trans. Electromagn. Compat.*, vol. 46, no. 4, pp. 512–528, Nov. 2004.
- [17] A. Maffucci, G. Miano, and F. Villone, "An enhanced transmission line model for conductors with arbitrary cross sections," *IEEE Trans. Adv. Packag.*, vol. 28, no. 2, pp. 174–188, May 2005.
- [18] A. Vukicevic, F. Rachidi, M. Rubinstein, and S. V. Tkachenko, "On the evaluation of antenna-mode currents along transmission lines," *IEEE Trans. Electromagn. Compat.*, vol. 48, no. 4, pp. 693–700, Nov. 2006.
- [19] Y. Wang *et al.*, "Evaluating field interactions between multiple wires and the nearby surface enabled by a generalized MTL approach," *IEEE Trans. Electromagn. Compat.*, vol. 60, no. 4, pp. 971–980, Aug. 2018.
- [20] Y. Wang, Y. S. Cao, D. Liu, R. W. Kautz, N. Altunyurt, and J. Fan, "A generalized multiple-scattering (GMS) method for modeling a cable harness with ground connections to a nearby metal surface," *IEEE Trans. Electromagn. Compat.*, vol. 61, no. 1, pp. 261–270, Feb. 2019.
- [21] Y. Wang, Y. S. Cao, D. Liu, R. W. Kautz, N. Altunyurt, and J. Fan, "Applying the multiple scattering (MS) method to evaluate the current response on a cable harness due to an incident plane wave," in *Proc. IEEE Int. Conf. Comput. Electromagn.*, Chengdu, China, 2018, pp. 1–3.

- [22] Y. S. Cao, Y. Wang, L. Jiang, A. E. Ruehli, J. Fan, and J. Drewniak, "Quantifying EMI: A methodology for determining and quantifying radiation for practical design guidelines," *IEEE Trans. Electromagn. Compat.*, vol. 59, no. 5, pp. 1424–1432, Oct. 2017.
- [23] J. Li, Y. Zhang, D. Liu, A. Bhobe, J. L. Drewniak, and J. Fan, "Radiation physics from two-wire transmission lines," in *Proc. IEEE Symp. Elec*tromagn. Compat. Signal Integrity, Santa Clara, CA, USA, Mar. 2015, pp. 160–164.
- [24] Y. S. Cao, L. Jiang, and A. E. Ruehli, "Distributive radiation and transfer characterization based on the PEEC method," *IEEE Trans. Electromagn. Compat.*, vol. 57, no. 4, pp. 734–742, Aug. 2015.
- [25] EMCoS: EMC Studio, Version 2018, 2018. [Online]. Available: http://www.emcos.com
- [26] J. Li and J. Fan, "Radiation physics and design guidelines of high-speed connectors," *IEEE Trans. Electromagn. Compat.*, vol. 58, no. 4, pp. 1331–1338, Aug. 2016.
- [27] Y. Leviatan and A. Adams, "The response of a two-wire transmission line to incident field and voltage excitation, including the effects of higher order modes," *IEEE Trans. Antennas Propag.*, vol. AP-30, no. 5, pp. 998–1003, Sep. 1982.
- [28] T. Nakamura, N. Hayashi, H. Fukuda, and S. Yokokawa, "Radiation from the transmission line with an acute bend," *IEEE Trans. Electromagn. Compat.*, vol. 37, no. 3, pp. 317–325, Aug. 1995.
- [29] F. Middelstaedt, S. V. Tkachenko, R. Rambousky, and R. Vick, "High-frequency electromagnetic field coupling to a long, finite wire with vertical risers above ground," *IEEE Trans. Electromagn. Compat.*, vol. 58, no. 4, pp. 1169–1175, Aug. 2016.
- [30] F. Rachidi and S. Tkachenko, Electromagnetic Field Interaction With Transmission Lines: From Classical Theory to HF Radiation Effects. Southampton, U.K.: WIT Press, 2008.
- [31] S. Chabane, P. Besnier, and M. Klingler, "A modified enhanced transmission line theory applied to multiconductor transmission lines," *IEEE Trans. Electromagn. Compat.*, vol. 59, no. 2, pp. 518–528, Apr. 2017.
- [32] S. Jin et al., "Analytical equivalent circuit modeling for BGA in high-speed package," *IEEE Trans. Electromagn. Compat.*, vol. 60, no. 1, pp. 68–76, Feb. 2018.
- [33] S. Jin, D. Liu, Y. Wang, B. Chen, and J. Fan, "Parallel plate impedance and equivalent inductance extraction considering proximity effect by a modal approach," *IEEE Trans. Electromagn. Compat.*, vol. 60, no. 5, pp. 1481– 1490, Oct. 2018.



Yansheng Wang (S'11–M'18) received the B.S. degree from Beihang University, Beijing, China, in 2012, and the Ph.D. degree from the Electromagnetic Compatibility Laboratory, Missouri University of Science and Technology, Rolla, MO, USA, in 2018, both in electrical engineering.

His research interests include radiation and immunity characterization for cable harness inside vehicle shell, method of moments, multiple-input multiple-output over-the-air testing, source reconstruction from near field and far field, desense measurement

and simulation, radio frequency interference, broadband E-/H-field probe design, conducted emission modeling, radiated source modeling, stochastic modeling for high-speed channels, and generic model development for PCIe3/4.



Ying S. Cao (S'14–M'16) received the B.S. degree in physics from the University of Science and Technology of China, Hefei, China, in 2012, and the Ph.D. degree in electrical engineering from the University of Hong Kong, Pokfulam, Hong Kong, in 2016.

Since October 2016, she has been a Visiting Assistant Research Professor with the Electromagnetic Compatibility (EMC) Laboratory, Missouri University of Science and Technology, Rolla, MO, USA. Her research interests include electromagnetic interference/polarization integrity/severity integrity, com-

putational electromagnetics, and multiphysics modeling.

Dr. Cao was the recipient of the 2016 IEEE EMC Symposium President's Memorial Award, the Best Student Symposium Paper Award at the 2016 IEEE International Symposium on EMC, Ottawa, ON, Canada, and the 2016 Applied Computational Electromagnetics Society Best Student Paper Award (fifth place).



**Dazhao Liu** (M'16) received the B.S. degree from Tsinghua University, Beijing, China, in 2008, and the M.S. and Ph.D. degrees from the Missouri University of Science and Technology (formerly University of Missouri-Rolla), Rolla, MO, USA, in 2010 and 2013, respectively, all in electrical engineering.

He is currently working in Silicon Valley, San Francisco Bay, CA, USA. His research interests include signal integrity, power integrity, electrostatic discharge, advanced measurement, and method of moments.



**Nevin Altunyurt** received the Ph.D. degree in electrical and computer engineering from the Georgia Institute of Technology, Atlanta, GA, USA, in 2010.

She was a Packaging Engineer with Intel Corporation between 2010 and 2013. She has been an Electromagnetic Compatibility (EMC) Research Engineer with Ford Motor Company, Dearborn, MI, USA, since 2013. Her research interests include system-level EMC simulations, wireless power transfer systems, and electromagnetic field exposure assessment.

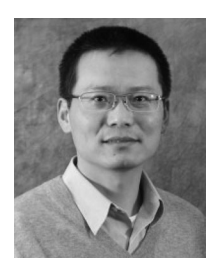


**Richard W. Kautz** received the M.S.E.E. degree with specialization in electromagnetics from The Ohio State University, Columbus, OH, USA, in 1984.

During 1981–1984, he was a Graduate Research Associate with The Ohio State University Electro-Science Lab, working on radar cross-sectional analysis. Upon graduation, he joined the Ford Motor Company, Dearborn, MI, USA, with vehicle electromagnetic compatibility (EMC) test development responsibilities. Since 2006, he has been with the Electric Machine Drive Systems Department, Ford

Research and Advanced Engineering, leading the development of numerical EMC and electromotive force (EMF) analysis methods for vehicle electrical systems, with an emphasis on electrified vehicle propulsion systems.

Mr. Kautz is active in Society of Automotive Engineers committees for EMC, the IEC TC 106/PT 62764 committee for vehicle EMF measurement, and is a Co-Chair of the J2954 Vehicle Wireless Charging EMC/EMF Subteam.



**Jun Fan** (S'97–M'00–SM'06–F'16) received the B.S. and M.S. degrees from Tsinghua University, Beijing, China, in 1994 and 1997, respectively, and the Ph.D. degree from the Missouri University of Science and Technology (formerly University of Missouri-Rolla), Rolla, MO, USA, in 2000, all in electrical engineering.

From 2000 to 2007, he was a Consultant Engineer with NCR Corporation, San Diego, CA, USA. In July 2007, he joined the Missouri University of Science and Technology (formerly University of Missouri-

Rolla), where he is currently a Professor and Director of the Missouri S&T Electromagnetic Compatibility (EMC) Laboratory. He also serves as the Director of the National Science Foundation Industry/University Cooperative Research Center for EMC and a Senior Investigator of the Missouri S&T Material Research Center. His research interests include signal integrity and electromagnetic interference (EMI) designs in high-speed digital systems, dc power-bus modeling, intrasystem EMI and RF interference, printed circuit board noise reduction, differential signaling, and cable/connector designs.

Dr. Fan served as the Chair of the IEEE EMC Society TC-9 Computational Electromagnetics Committee from 2006 to 2008. He was a Distinguished Lecturer of the IEEE EMC Society in 2007 and 2008. He currently serves as the Chair of the Technical Advisory Committee of the IEEE EMC Society. He is an Associate Editor for the IEEE TRANSACTIONS ON ELECTROMAGNETIC COMPATIBILITY and *EMC Magazine*. He received the IEEE EMC Society Technical Achievement Award in Aug. 2009.